Magnetic Resonance in Medicine 41:2–7 (1999)

Inverse Correlation Between Choline Magnetic Resonance Spectroscopy Signal Intensity and the Apparent Diffusion Coefficient in Human Glioma

Rakesh K. Gupta,[1] Usha Sinha,[1] Timothy F. Cloughesy,[2,4] and Jeffry R. Alger[1,3,4]*

Magnetic resonance spectroscopy and diffusion magnetic resonance imaging (MRI) characteristics of human intracranial glioma were studied. Present knowledge suggests a hypothetical inverse relationship between the characteristic choline signal intensity elevation and the apparent diffusion coefficient (ADC) in glioma. Twenty cases of glioma were examined with diffusion-weighted echoplanar imaging and proton magnetic resonance spectroscopic imaging (^{1}H-MRSI). A statistically significant inverse correlation between the choline signal intensity and the ADC was found ($P = 0.0004$) in radiologically defined tumor-containing regions. This study is the first in which diffusion MRI and ^{1}H-MRSI were used to evaluate human intracranial glioma jointly. It provides insight into how to interpret choline signal intensity elevation in terms of tumor cellularity and proliferative potential when ADC images are also available. Magn Reson Med 41:2–7, 1999. © **1999 Wiley-Liss, Inc.**

Key words: brain; tumor; glioma; magnetic resonance imaging; magnetic resonance spectroscopy; diffusion

Proton magnetic resonance spectroscopic imaging (^{1}H-MRSI) has utility in the diagnosis and management of human intracranial glioma. Previous studies have demonstrated that prebiopsy spectroscopic signal readings from intracranial glioma can predict the histopathological diagnosis (1), and that increases in the choline spectroscopic signal intensity accompany malignant degeneration (2–4). However, in interpreting ^{1}H-MRSI findings, one must consider that human glioma is characterized by topographically heterogeneous histopathology. A single glioma can display regions of tumor-infiltrated brain tissue, regions containing a high density of tumor cells, and necrotic regions. Edematous brain tissue can also surround the tumor. These histopathologically unique regions are expressed to a highly variable extent in different patients. This is particularly true in high-grade glioma such as glioblastoma multiforme. Moreover, the extent to which these histopathologically unique regions are expressed in a single patient can vary with time due either to natural tumor progression or to treatment. Spectroscopic findings, whether obtained for prediction of the histopathological diagnosis or for assessment of malignant degeneration, hypothetically should be influenced by the topographic histopathologic constitution. The dense hypercellular regions are expected to demonstrate the substantial choline signal intensity elevation characteristic of glioma (5), whereas other regions situated at the infiltrating margin or in the necrotic core are expected to demonstrate less choline signal intensity elevation. By the same reasoning, different patients who have the same histopathological diagnosis could hypothetically have different average choline signal elevations due to the variable extent to which necrosis is interspersed with dense cellularity. This reasoning suggests that the ^{1}H-MRSI signal alterations associated with glioma, particularly the extent of choline signal intensity elevation, will correlate with alternate and independent measures of the local cellularity. The study reported herein tests this hypothesis.

Diffusion magnetic resonance imaging (MRI) is thought to enable the identification of the unique histopathologic components of glioma that may not be clearly distinguishable on conventional MRI (6–9). Higher apparent diffusion coefficients (ADCs) are suggestive of low cellularity (cyst, necrosis or edema); lower ADC values suggest higher cellularity. Therefore, in this study, diffusion MRI is used to provide an alternate and independent measure of local cellularity. The hypothesis was tested by obtaining topographically correlated readings of the ADC and the choline signal intensity elevations in a group of glioma patients. For this initial investigation of the hypothesis, patients having a wide range of histopathologic diagnoses at various stages of management were purposely studied; there is no a priori reason to believe the hypothesis would not hold over such a group.

MATERIALS AND METHODS

Diffusion-weighted imaging (DWI) and ^{1}H-MRSI results of the first 20 brain tumor patients, who underwent these scans for clinically indicated purposes, were obtained from electronic archives. The patients (Table 1) had a variety of different histopathologic diagnoses and were at differing stages of treatment. This provided a wide interval of ADC and ^{1}H-MRSI readings over which to test the hypothesis. The patient group included 12 men and 8 women with ages

[1]Department of Radiological Sciences, University of California, Los Angeles, California 90095-1721.

[2]Department of Neurology, University of California, Los Angeles, California 90095-1721.

[3]Brain Research Institute, University of California, Los Angeles, California 90095-1721.

[4]Jonsson Comprehensive Cancer Center, University of California, Los Angeles, Los Angeles, California 90095-1721.

Grant sponsor: American Cancer Society; Grant number: EDT-119; Grant sponsor: National Cancer Institute; Grant number: CA 76524.

*Correspondence to: Jeffry R. Alger, Department of Radiological Sciences, UCLA Medical Center, BL-428 CHS, 10833 Le Conte Avenue, Los Angeles, CA 90095-1721. E-mail: jralger@ucla.edu

Received 2 March 1998; revised 24 August 1998; accepted 28 August 1998.

Table 1
Summary of Case Material

Patient	Pathology	Treatment
gp	GBM	RT + chemo
pd	LGA	None
md	AMG	RT + chemo
ws	GBM	RT + chemo
db	GBM	Presurgical
bb	*LGA	RT + chemo
gn	LGA	RT + chemo
ss	GBM	RT + chemo
wb	LGA	RT
bs	GBM	Presurgical
ha	GBM	RT + chemo
wl	GLGA	RT + chemo
ek	GBM	RT
kj	LGO	Presurgical
wr	GBM	RT + chemo
jm	AA	RT + chemo
jr	LGO	Post surgery
cm	GBM	Presurgical
rr	LGO	Presurgical
rm	AMG	Presurgical

GBM, glioblastoma multiforme; LGA, low-grade astrocytoma; AMG, anaplastic mixed glioma; GLGA, gemistocytic low-grade astrocytoma; LGO, low-grade oligodendroglioma; AA, anaplastic astrocytoma; RT, radiotherapy; chemo, chemotherapy; *LGA, progressive low-grade astrocytoma.

ranging from 27 to 68 years. All patients had histologically proven diagnoses. Six of the patients were undiagnosed and untreated (except for steroids) at the time of the scanning; these six patients went on to the surgeries, which provided histopathologic diagnoses, within 1 week of scanning.

The patients were scanned using a 1.5 T MRI system (Signa 5.x Echospeed, General Electric Medical Systems, Milwaukee, WI). Conventional MRI, ^{1}H-MRSI, and DWI were performed during the same scanning session without repositioning the patient. The conventional imaging included pre- and post-contrast T1-weighted axial imaging (TR/TE/NEX 500/8/2, slice thickness 3 mm, slice gap 0, 192 × 256 matrix) and fast spin-echo proton-density-weighted and T2-weighted axial imaging (TR/TE1/TE2/NEX 6000/14/126/2, slice thickness 3 mm, slice gap 0, 192 × 256 matrix). MRI contrast material (Magnevist, Berlex Laboratories, Wayne, NJ) was given after the ^{1}H-MRSI and DWI scanning.

Axial ^{1}H-MRSI was performed using a three-slice multislice technique with TR/TE 2300/272, 24 × 24 phase encoding array, slice thickness of 12 mm, and field of view 240 mm. This prescription provided proton magnetic resonance spectra from an array of voxels (nominal dimensions of 10 × 10 × 12 mm^3) from each of the three chosen slices. Water suppression was accomplished using three frequency-selective radiofrequency pulses in concert with gradient pulses to destroy coherent water magnetization at the beginning of the pulse sequence. Lipid suppression was achieved using the short-tau-inversion-recovery method with TI of 170 msec.

Diffusion-weighted echoplanar images were acquired using five b-values in each of three orthogonal gradient axes (10,11). To simplify image manipulation, diffusion scans were performed using 12 mm thick slices prescribed to match the ^{1}H-MRSI slice prescription. Key diffusion sensitization parameters were: diffusion gradient duration (δ) of 35 msec and diffusion time (Δ) of 38.7 msec along the read and phase axis and 43.2 msec along the slice-select axis. b values ranged from 0 to 939 sec/mm^2 for diffusion gradients along the read/phase axis and from 0.2 to 1112 sec/mm^2 for diffusion gradients applied along the slice select axis. The diffusion-weighted image acquisition used TE/TR/FOV 90 msec/3000 msec/24 cm at an in-plane resolution of 128 × 128. The diffusion-weighted images were interpolated to 256 × 256 using software provided by the manufacturer prior to presentation and analysis. ADC images were calculated from the diffusion-weighted images. Images acquired at the five values of the diffusion-sensitizing gradient in each direction were log-linear fit on a pixel-by-pixel basis to generate the ADC images: ADC_{xx}, ADC_{yy}, ADC_{zz}. The ADC trace image was then calculated as:

$$1/3[ADC_{xx} + ADC_{yy} + ADC_{zz}].$$

In the remainder of this paper, the ''ADC trace'' will be denoted as ''ADC.'' The ''b-value'' has contributions from imaging gradients, diffusion gradients, and the interaction between imaging and diffusion gradients (''cross-terms''). We included the contribution from the cross-term along the slice axis (z) only based on the following analysis. The sequence design was such that diffusion gradients were refocused before application of any imaging gradients along the read and phase directions. Thus cross-terms from imaging gradients along the read and phase directions were eliminated. The crusher gradients flanking the refocusing pulse contributed an average value of 5% to the total b-value. The signal intensity's dependence on diffusion is given by

$$\ln [S(b)/S(b = 0))] = -\sum_{i=x,y,z}\sum_{j=x,y,z}(b_{ij}ADC_{ij}),$$

where S(b) is the signal in the presence of diffusion gradients and S(b = 0) is the signal in the absence of any diffusion gradients. b_{ij} and ADC_{ij} are the elements of the b-matrix and diffusion tensor, respectively. Signal attenuation effects arising from the imaging gradients alone along any direction are not considered since they are present in both the S(b) and S(b = 0) data. Since the only substantial cross-term is that from the crusher gradients along the z (slice)-axis, the diffusion equation reduces to

$$\ln [(S(b)/S(b = 0))] = -(b_{yy}ADC_{yy} + 2b_{yz}ADC_{yz}) \quad \text{(y-axis)}$$

$$\ln [(S(b)/S(b = 0))] = -(b_{xx}ADC_{xx} + 2b_{xz}ADC_{xz}) \quad \text{(x-axis)}$$

$$\ln [(S(b)/S(b = 0))] = -(b_{zz}ADC_{zz}) \quad \text{(z-axis).}$$

Here, the b_{zz} term explicitly includes the contribution from the imaging-diffusion ''cross-term.'' However, the second term in the diffusion equation along the x and y-axis was neglected. The contribution from this term was less than

1% of the total signal attenuation due to the combination of a small cross-term and a small off-diagonal term. This enabled us to estimate the trace without the full tensor calculation.

The ^{1}H-MRSI data were Fourier reconstructed following sine-bell spatial filtering and 2.0 Hz lorentzian time domain filtering to form an two-dimensional array of voxel frequency spectra from each of the three imaged slices. The tissue location that produced each voxel frequency spectrum could be identified on any of the topographically correlated MRIs, including the ADC image. Frequency spectra from each of the intracranial voxels were frequency-referenced by identifying characteristic spectroscopic signals, and then baseline corrected. Integrated magnitude signal intensities (hereafter referred to as ''signal intensities'') of the choline and N-acetyl aspartate (NAA) signals were obtained by integration of a 0.1 ppm region around the respective signal maxima. Signal intensities were color coded for display in the figure. Choline signal alterations associated with tumor were quantitated using the ''normalized choline'' signal approach (2,3,12). The choline signal intensities in spectroscopic imaging voxels located in tumor-containing regions were read. Readings were also made from voxels located in contralateral normal-appearing regions, and the ratio (nCho) of the tumor to contralateral signal intensity was calculated for each patient. The nCho ratio was used in the statistical analysis.

Conventional MRI scans were used to identify the voxel locations as being composed of tumor or of normal tissue. ADC values were read from the computed 256 × 256 ADC images, which were matched in slice location and slice thickness with the ^{1}H-MRSI prescription. The mean ADC values produced by volumes having the same location and size (10 × 10 × 12 mm^3) as those taken for the ^{1}H-MRSI choline signal intensity readings were used. The ratio of tumor tissue ADC to contralateral normal tissue ADC was used to maintain consistency with the ^{1}H-MRSI quantitation. ^{1}H-MRSI and ADC readings were taken from 62 tumor and corresponding normal voxels from the 20 patient studies. The sampled tumor containing regions included those having characteristic appearances (on conventional MRI) of edema, necrosis, cystic cavity, and solid tumor. Data were modeled with correlation statistics using a commercially available statistical program (JMP, SAS Institute).

RESULTS

Typical imaging and spectroscopic findings are presented in Fig 1, which illustrates presurgical findings from a newly diagnosed case of oligodendroglioma of the left temporoparietal region. The conventional T2-weighted and postcontrast MR images demonstrate a heterogeneous lesion composed of a T2-weighted hypointense mass showing modest contrast enhancement surrounded by tissue demonstrating T2-weighted hyperintensity and a probable cystic cavity. On the ADC image, the lesion demonstrates heterogeneity; the central T2-weighted hypointense mass is surrounded by more hyperintense-appearing tissue. Spectroscopic imaging results demonstrate a reduced NAA signal intensity throughout the lesion, consistent with the destruction of neuronal architecture, although the choline signal intensity appears to be elevated in a topographically heterogeneous manner. Choline signal intensity is elevated in the central mass, and this elevation extends anteriomedially into the region that shows T2-weighted and ADC hyperintensity. Plots of voxel spectra are provided in Fig 1B–E. In these figures, the location of the voxel that generated the spectrum is shown on the ADC image. These figures illustrate an inverse relationship between the ADC readings and the extent of choline signal intensity elevation. The central mass shows the most hypointense ADC reading and the greatest choline signal intensity elevation (Fig 1C), while voxels demonstrating more ADC hyperintensity show smaller choline signal intensities.

Results from the entire patient group are summarized in Figure 2, which illustrates a general association of low ADC readings with high choline signal intensities readings

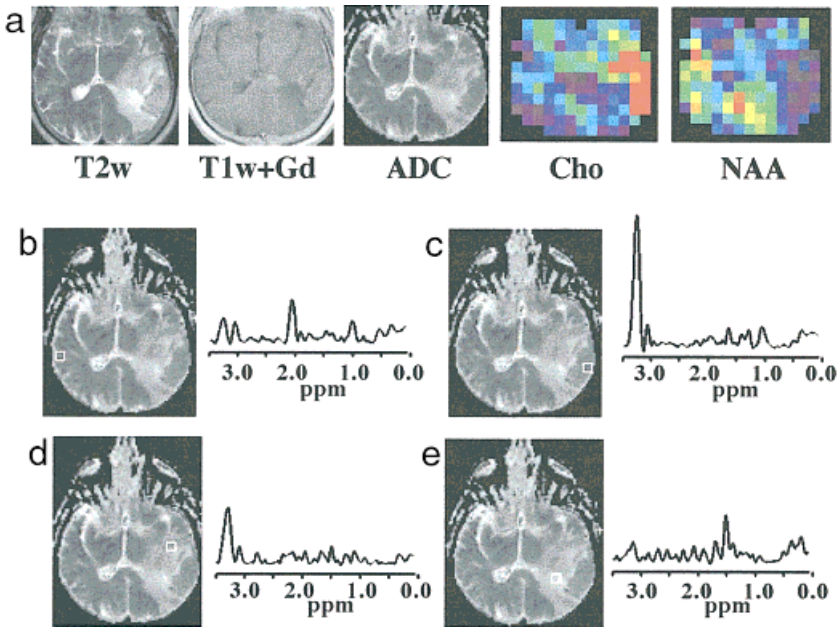

FIG. 1. Illustrative image and spectroscopy findings from one of the cases. **A:** Conventional MR images together with ADC and spectroscopic images (Cho and NAA) from a single 12 mm thick slice. The Cho and NAA spectroscopic images are displayed using identical color tables in which warmer colors denote higher signal intensity. The spectroscopic images are displayed at their nominal in-plane voxel resolution (10 × 10 mm^2). **B–E:** Magnitude spectra arising from the nominal volume element shown on the ADC image to the left of each spectrum. Vertical scaling for all displayed spectra are identical so that signal intensity differences between voxels may be readily appreciated. Signal assignments in the spectra (referred to the chemical shift axis provided with each spectrum) are: choline (3.25 ppm), creatine (3.0 ppm), NAA (2.0), lactate/lipid (1.0–1.5 ppm).

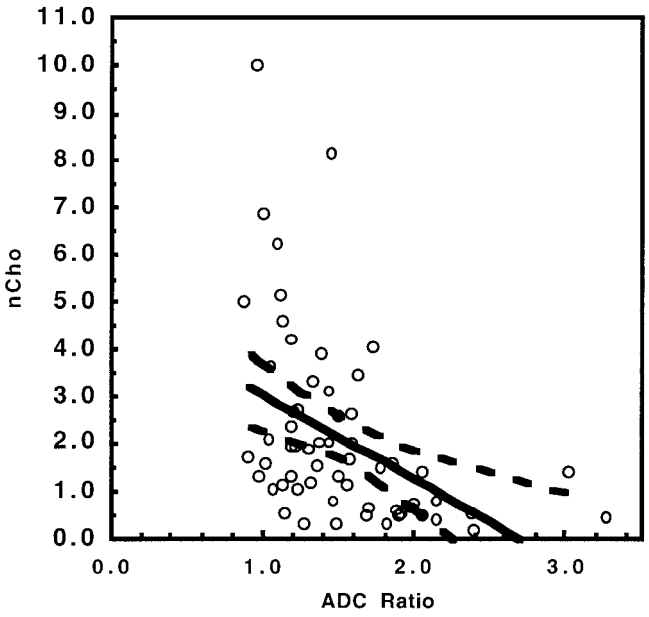

FIG. 2. Correlation plot of normalized choline (the ratio of tumor choline to contralateral choline signal intensity) versus the ADC tumor to contralateral ratio. The solid line represents the best linear fit to the data. The fitting was performed using ANOVA linear regression modeling as provided by JMP software. The dashed lines display the 95% confidence interval for the linear regression fit.

and vice versa. Statistical linear regression modeling supports rejection ($P = 0.0004$) of the null hypothesis that the data are characterized by a line of zero slope. This evidence supports the hypothesis of a statistically significant inverse correlation between ADC and choline signal intensity, although there is no a priori reason to hypothesize a linear relationship between the parameters. The hypothesis was also tested using several different ways of expressing the choline spectroscopy and diffusion characteristics (data not shown). One may use any consistent MR signal obtained during the same examination as a intersubject calibration factor to express choline signal intensity. One such consistent signal is the MRI signal intensity from unaffected white matter. The parametric ADC value inversely correlated with choline signal intensity referenced to normal white matter MRI signal intensity ($P = 0.005$). The side-to-side ADC ratio also inversely correlated with the same ratiometric measure of choline signal intensity ($P = 0.003$).

The data were generated by a variety of tumors having different pathological characteristics at various stages of evaluation and treatment. Efforts to isolate sub-relationships between ADC and choline signal intensity readings in subgroups having particular pathological or treatment characteristics were mostly unsuccessful in this small study population. However, when only cases of glioblastoma multiforme were considered, statistically significant ($P < 0.05$) inverse correlations between either ADC measure (ratiometric or parametric) and either choline measure (contralateral normalization or white matter MRI normalization) were obtained. This is a topic of presently ongoing observations.

Although the correlation illustrated in Fig. 2 is statistically significant, ''outliers'' showing relatively high choline signal intensity readings are apparent. Several readings showing near normal ADC ratios (1.0–1.2) suggestive of cellularity presented uncharacteristically high normalized choline signal intensity ratios ranging from 6.0 to 12.0.

DISCUSSION

Previous studies in which human intracranial glioma has been examined with diffusion imaging (6–9) have inferred from the radiological appearance of the tumors that ADC provides an indication of the relative intracellular and extracellular volumes within the tissue being examined. High ADC values were attributed to necrosis and cyst while lower values approaching those seen in normal tissue were attributed to dense highly cellular tumor tissue. This inference is consistent with diffusion imaging findings in acute human stroke. One of the more plausible explanations for the ADC decrease seen in acutely ischemic brain tissue is that the failure of energy production results in ion balance disturbances and the redistribution of water from the extracellular to the intracellular medium (11). The volume redistribution leads to a reduced volume average ADC because the intracellular medium is more viscous and contains more barriers to Brownian diffusion compared with the extracellular medium (11). The present case material suggests that even the more cellular portions of intracranial glioma tend to display somewhat higher ADC values compared with normal tissue. Most of the tumor ADC readings were greater than those obtained from normal tissue in the contralateral hemisphere. This is consistent with the presence of a relatively large extracellular volume associated with micronecrosis and interstitial edema even in the more cellular tumor components.

Essentially all previous clinical proton ^{1}H-MRS examinations of human glioma have noted that the choline ^{1}H-MRS signal intensity appears to be elevated. Indeed, the elevation of the choline signal intensity seen in ^{1}H-MRS or the phosphocholine signal intensity seen in ^{31}P-MRS seems to be a characteristic of neoplastic tissue. Early ^{31}P-MRS studies of neoplastic tissues and cells identified elevated phospomonoesters and attributed this to active cell proliferation (13,14). Subsequent ^{31}P-MRS studies of cell cultures have been somewhat confirmatory. Aiken and Gillies (15) demonstrated a consistent and dramatically lower phosphocholine/phosphoethanolamine (PCho/PEtn) ratio in stationary cultures compared with actively proliferating cultures of human cells and human tumor cells. In a study of rat glioma cell cultures, Gillies et al (16) concluded that that there is a decrease in the biosynthesis of PCho concomitant with a reduction in culture growth. Similarly, in a study of murine mammary carcinoma cultures during irradiation, Mahmood et al (17) found a strong radiation dose-dependent response in the relative PCho/PEtn ratio, suggesting that changes in the PCho levels may be related to alterations in cell proliferation. Aiken et al (18) found that mitogenic stimulation of rat-2 fibroblasts resulted in a significant increase in the uptake of a phosphonium choline into the phosphomonoester pool, suggesting that growth stimulation leads to an increase in the PCho levels. The association of PCho increases with cellular proliferation is often attributed to acceleration of membrane and phospholipid metabolism, given that PCho is a crucial

biosynthetic precursor of membrane phospholipids. Therefore, the PCho level is likely to be elevated because of the enhanced membrane synthetic needs of actively proliferating cells. Taken together, many of the studies noted demonstrate that PCho is elevated in actively proliferating cells and that this can be measured non-invasively with either ^{31}P- or ^{1}H-MRS.

Bakoo et al (19) have sought to determine whether the spectroscopically detectable alterations in cellular levels of choline, PCho, and glycerophosphocholine (GPCho) are a reflection of rapid cell division or are specifically related to oncogenic transformation. In fully transformed rapidly proliferating Schwann cells, total choline (=choline + PCho + GPCho) expressed relative to total protein was not significantly different compared with normal cells, although the PCho level (expressed relative to total protein) was significantly increased. By comparing choline metabolite assays from different cell types with differing doubling times (some of which were oncogenically transformed), Bakoo et al (19) found that neither the total choline metabolite level, nor the PCho level, nor the PCho/GPCho ratio was associated with the proliferation rate. Nevertheless, their data emphasize the significant probability of an association between oncogenic transformation and the PCho/GPCho ratio.

Interpretation of our results within the context of Bakoo et al's (19) is complicated by three study design differences. First, it has not been possible with in vivo spectroscopic techniques to resolve PCho, choline, and GPCho signals. Choline signals measured in the present study are thereby equivalent to the ''total choline'' measured by Bakoo et al (19). Their study predicts no relationship between the measured in vivo total choline signal and proliferation. This is by no means inconsistent with our findings, which make a relatively weak case for a relationship between proliferation rate and total choline levels (see below). Moreover, our inability to resolve components of the total choline signal makes it impossible to evaluate whether there is consistency with any previous findings related to the PCho/GPCho ratio. Second, in vivo spectroscopy lacks a convenient measurable parameter analogous to ''mg total protein'' that can be used to express the cellular density within the spectroscopically sampled volume. ADC readings may well provide this (see below). Third, the relevance of the transformed Schwann cell model to human intracranial glioma is far from clear. For example, three glioblastoma lines studied by Bakoo et al (19) produced PCho, GPCho, and total choline levels that appeared to be quite different compared with fully transformed Schwann cells. These lines also produced highly variable PCho/GPCho ratios having a mean value 64% higher than that observed in the fully transformed Schwann cells. Although Bakoo et al (19) provided insufficient data to assess the statistical significance of these apparent differences, their glioblastoma findings suggest that caution should be exercised in extrapolation to clinically encountered cancers other than Schwannoma. Bakoo et al's (19) glioblastoma findings support the concept (discussed more fully below) that the choline signal observed in glioblastoma (which accounted for about half of our cases) is primarily due to PCho.

In ^{1}H-MRS studies of human brain tumors that were correlated with histopathological readings, Chang et al (20) and Miller et al (21) found that the ^{1}H-MRS choline signal is produced mostly by PCho but also depends on the local cellularity in consistency with PCho being an intracellular metabolite. These two studies strongly emphasize the combined influences of tumor cellularity and choline metabolite levels on ^{1}H-MRS readings of the choline signal intensity elevation. One must consider that the choline signal may be elevated because the sampled tumor region is highly cellular or because the cells in the sampled volume display a high intracellular PCho level that may be associated with enhanced proliferative potential (13–18) or with oncogenic transformation (19). Of course, from a biological perspective, these tumor characteristics may be related; one may logically argue that tissue that displays a high proliferative potential or that is oncogenically transformed is also likely to display high cellularity in the absence of compensating apoptotic mechanisms or limitations of vascular supply.

The merging lines of investigation from diffusion MRI and MRS, discussed in the preceding paragraphs, suggest the hypothesis of an inverse correlation between ADC readings and choline signal intensity elevation in glioma. This hypothesis was tested, and statistically significant support for it was obtained in the present study. On average, regions that showed higher ADC readings (presumably those of low cellularity) tended to show less pronounced choline signal elevation, while regions showing lower ADC (presumably those of higher cellularity) produced stronger choline signal intensity. The inverse correlation suggests that the tumor cell density plays a major role in defining the level of choline signal elevation measured by ^{1}H-MRSI. The finding argues that if choline signal elevation reports proliferative potential, it does so only through the fact that proliferation leads to cellularity. If the inverse correlation were perfect, one could use diffusion imaging instead of proton spectroscopy. However, the inverse correlation shown in Fig. 2 is imperfect. Some of the tumor voxels that appeared to have a relatively high cellularity based on ADC measures also showed uncharacteristically high choline signal elevations. These ''outliers'' may well be the very aggressive tumor voxels that display both high cellularity and high proliferative potential. Admittedly, this speculation hinges on the outcome of the unresolved debate (13–20) about whether total spectroscopically measured total choline levels in glioma, even after cell density is accounted for, should depend on proliferative potential. Nevertheless, it is appealing to consider that such ''aggressivity'' information conceivably has distinct far-reaching prognostic and therapeutic significance, leading to the conclusion that diffusion MRI and MRS may indeed complement each other when intracranial glioma is assessed.

The characteristic well-known limitations of ^{1}H-MRSI are present in this study. The spectroscopic imaging measurements used substantial T2 weighting. Therefore, the spectroscopic signal intensities were influenced by T2 and by the concentration of the signal-producing nuclei. This methodology was chosen because it reliably produces topographic measures of clinically relevant signal intensities and is consistent with that used by at least two other

groups (1,4) who have evaluated cerebral neoplasia using spectroscopic imaging techniques. Because T2-weighted spectroscopic imaging was used, one cannot rule out that the choline signals arising from the various tissues have differing T2s that influence the findings. A follow-up study using single volume techniques, which can be reliably applied in the short-TE regime, would be the most appropriate way of investigating this possibility. Spectroscopic signal intensities are quantified using ratios, rather than absolute quantitative measures of concentration. The ^{1}H-MRSI volume resolution is lower than for either conventional MRI or diffusion MRI due to signal-to-noise ratio limitations, the need for two-dimensional phase encoding, and the point spread characteristic of low-resolution Fourier imaging. Despite these limitations, statistically significant support for a hypothesis having substantial clinical and biological significance was obtained.

This study is the first in which diffusion MRI and MRS were used jointly to evaluate human intracranial glioma. It demonstrates a statistically significant inverse correlation between ADC readings and choline signal intensity elevation. It also provides insight into how to interpret choline signal intensity elevation in terms of tumor cellularity and proliferative potential when ADC images are also available.

REFERENCES

1. Preul MC, Caramanos Z, Collins DL, Villemure JG, Leblanc R, Olivier A, Pokrupa R, Arnold DL. Accurate, noninvasive diagnosis of human brain tumors by using proton magnetic resonance spectroscopy. Nature Med 1996;2:323–325.
2. Tedeschi G, Lundbom N, Raman R, Bonavita S, Duyn JH, Alger JR, Di Chiro G. Increased choline signal coincides with malignant degeneration of cerebral gliomas: a serial proton magnetic resonance spectroscopic imaging study. J Neurosurg 1997;8:516–524.
3. Fulham MJ, Bizzi A, Dietz MJ, Shih HH, Raman R, Sobering GS, Frank JA, Dwyer AJ, Alger JR, Di Chiro G. Mapping of brain tumor metabolites with proton MR spectroscopic imaging: clinical relevance. Radiology 1992;185:675–686.
4. Wald LL, Nelson SJ, Dey MR, Noworolski SE, Henry RG, Huhn SL, Chang S, Prados MD, Sneed PK, Larson DA, Wara WM, McDermott M, Dillon WP, Gutin PH, Vigneron DB. Serial proton magnetic resonance spectroscopy imaging of glioblastoma multiforme after brachytherapy. J Neurosurg 1997;87:525–534.
5. Gill SS, Thomas DG, Van Bruggen N, Gadian DG, Peden CJ, Bell JD, Cox IJ, Menon DK, Iles RA, Bryant DJ. Proton MR spectroscopy of intracranial tumours: in vivo and in vitro studies. J Comput Assist Tomogr 1990;14:497–504.
6. Brunberg JA, Chenevert TL, McKeever PE, Ross DA, Junck LR, Muraszko KM, Dauser R, Pipe JG, Betley AT. In vivo MR determination of water diffusion coefficients and diffusion anisotropy: correlation with structural alteration in gliomas of the cerebral hemispheres. AJNR 1995;16:361–371.
7. Krabbe K, Gideon P, Wagn P, Hansen U, Thomsen C, Madsen F. MR diffusion imaging of human intracranial tumors. Neuroradiology 1997; 39:483–489.
8. Yanaka K, Shirai S, Kimura H, Kamezaki T, Matsumuna A, Nose T. Clinical application of diffusion-weighted magnetic resonance imaging to intracranial disorders. Neurol Med Chr (Tokyo) 1995;35:648–654.
9. Tien RD, Felsberg GL, Friedman H, Brown M, MacFall J. MR imaging of high grade cerebral gliomas: value of diffusion weighted echoplanar pulse sequences. AJR 1993;162:671–677.
10. Le Bihan D, Turner R, Douek P. Is water diffusion restricted in human brain white matter? An echo-planar NMR imaging study. Neuroreport 1993;7:887–890.
11. Warach S, Gaa J, Stiewart B, Wielopolski F, Edelman RR. Acute human stroke studied by whole brain echo planar diffusion-weighted magnetic resonance imaging. Ann Neurol 1995;37:231–241.
12. Lazareff JA, Olmstead C, Bockhorst KH, Alger JR. Proton magnetic resonance spectroscopic imaging of pediatric low-grade astrocytomas. Childs Nerv Syst 1996;12:130–135.
13. Daly PF, Cohen JS. Magnetic resonance spectroscopy of tumors and potential in vivo clinical applications: a review. Cancer Res 1989;49:770–779.
14. Daly PF, Lyon RC, Faustino PJ, Cohen JS. Phospholipid metabolism in cancer cells monitored by 31P NMR spectroscopy. J Biol Chem 1987;262: 14875–148758.
15. Aiken NR, Gillies RJ. Phosphomonoester metabolism as a function of cell proliferative status and exogenous precursors. Anticancer Res 1996;16:1393–1397.
16. Gillies RJ, Barry JA, Ross BD. In vitro and in vivo 13C and 31P NMR analyses of phosphocholine metabolism in rat glioma cells. Magn Reson Med 1994;32:310–318.
17. Mahmood U, Alfieri AA, Thaler H, Cowburn D, Koutcher JA. Radiation dose-dependent changes in tumor metabolism measured by 31P nuclear magnetic resonance spectroscopy. Cancer Res 1994;54:4885–4891.
18. Aiken NR, Szwergold ES, Kappler F, Stoyanova R, Kuesel AC, Shaller C, Brown TR. Metabolism of phosphonium choline by rat-2 fibroblasts: effects of mitogenic stimulation studied using ^{31}P NMR spectroscopy. Anticancer Res 1996;16:1357–1363.
19. Bhakoo KK, Williams SR, Florian CL, Land H, Noble MD. Immortalization and transformation are associated with specific alterations in choline metabolism. Cancer Res 1996;56:4630–4635.
20. Chang L, McBride D, Miller BL, Cornford M, Booth RA, Buchthal SD, Ernst TM, Jenden D. Localized in vivo ^{1}H magnetic resonance spectroscopy and in vitro analyses of heterogeneous brain tumors. J Neuroimaging 1995;5:157–163.
21. Miller BL, Chang L, Booth R, Ernst T, Cornford M, Nikas D, McBride D, Jenden DJ. In vivo ^{1}H MRS choline: correlation with in vitro chemistry/histology. Life Sci 1996;58:1929–1935.